Influence of Monomer Feeding on a Fast Cold Nanoparticles Synthesis: Time-Resolved XANES and SAXS Experiments

ARTICLE *in* LANGMUIR · SEPTEMBER 2010

Impact Factor: 4.46 · DOI: 10.1021/la1020274 · Source: PubMed

5 AUTHORS, INCLUDING:

Benjamin Abecassis
French National Centre for Scientific Research
30 PUBLICATIONS **600** CITATIONS
SEE PROFILE

Fabienne Testard
Atomic Energy and Alternative Energies Com…
52 PUBLICATIONS **1,068** CITATIONS
SEE PROFILE

Qingyu Kong
Argonne National Laboratory
65 PUBLICATIONS **1,135** CITATIONS
SEE PROFILE

Langmuir
Article
pubs.acs.org/Langmuir

Influence of Monomer Feeding on a Fast Gold Nanoparticles Synthesis: Time-Resolved XANES and SAXS Experiments

Benjamin Abécassis,[†,§] Fabienne Testard,[†] Quingyu Kong,[‡] Baudelet Francois,[‡] and Oliver Spalla*[,†]

[†]*CEA Saclay, DSM/IRAMIS/UMR 3299 CEA/CNRS SIS2M/Laboratoire Interdisciplinaire sur l'Organisation Nanométrique et Supramoléculaire, 91191 Gif sur Yvette, France, and* [‡]*Synchrotron SOLEIL, L'Orme des Merisiers Saint-Aubin, BP 48 91192 Gif sur Yvette Cedex, France.* [§]*Current address: MMN, UMR Gulliver, ESPCI, 10, rue Vauquelin, 75005 Paris, France.*

Received May 19, 2010. Revised Manuscript Received July 19, 2010

A comprehensive study of the mechanism of gold nanoparticle formation has been conducted using third-generation synchrotrons. The particles were obained by reduction of $AuCl_3$ by BH_4^- in toluene. Gold oxidation state was monitored by X-ray absorption near edge spectroscopy (XANES), while the size and concentration of the nanoparticles were assessed by small-angle X-ray scattering (SAXS). A time-resolution of 100 ms has been achieved for a total formation time of a few seconds. The change with time of the total amount of Au(0) present in the solution is obtained by XANES. The change of the amount of Au(0) inside the nanoparticles is obtained from the SAXS signal. The comparison between these two quantities shows that a measurable amount of Au(0) exists transiently as monomers (or very small entities) in solution and this quantity is linked to an observed burst of nucleation of nanoparticles. The reduction kinetics is strongly influenced by the presence of ligands and a change in temperature. A model coupling the observed reduction kinetics and nucleation and growth laws is able to recover the final size and number densities of the explored experimental conditions.

Introduction

Due to their potential applications, the synthesis of nanoparticles has been widely studied over the past decade,[1,2] taking advantage of the long history of colloidal chemistry and physics. Despite these efforts, the mechanism of nanoparticle formation in liquid media remains difficult to ascertain. Though control over size and shape of nanoparticles is becoming more and more accurate, trial and error is still the method of choice to discover and optimize new syntheses. A better understanding of the effect of the different experimental parameters would pave the way for retrosynthesis-like strategies in inorganic nanoparticle synthesis and hence result in a finer control over the complexity of the resulting product. The formation of nanoparticles from a mixture of several chemical compounds is still a matter of debate. The rapid transition between initial reactants and monomers and the characterization of the nuclei (concentration, shape, and size) with time is difficult to probe. The growth of the nuclei by addition of monomers or agglomeration can be separated in time or can be partially simultaneous with the nucleation stage. The lack of reliable experimental data persists as these transient events are difficult to probe in situ by conventional, widely spread techniques such as electronic microscopy. Most of the time, reactions occur over a few seconds, hindering the possibility of quenching for further analysis. A complete description of the formation mechanism would require measuring, with a sufficient time resolution, the different product concentrations during the course of the reaction as well as the number and size distribution of the nanoparticles. In this respect, small angle X-ray scattering (SAXS) is perfectly suited for assessing the nanoparticle's properties (size, shape, and polydispersity),[3−15] and X-ray absorption is very sensitive to chemical speciation. With recent improvements in instrumentation (synchrotrons of third generation), SAXS can be coupled with a stopped flow or continuous flow apparatus to follow the nucleation and growth of gold nanoparticles with a time resolution from seconds[16,17] down to a few tens of milliseconds.[6,16,18] A recently described jet technique[13] was used for the microsecond time scale. A quantitative fitting of the scattering diagram at the absolute scale allowed to determine the concentration, size, and distribution of the first nuclei and to follow their subsequent growth.[6] X-ray absorption near edge

*To whom correspondence should be addressed. E-mail: olivier.spalla@cea.fr.

(1) Tao, A.; Habas, S.; Yang, P. *Small* **2008**, *4*, 310–325.
(2) Kwon, S.; Hyeon, T. *Acc. Chem. Res.* **2008**, *41*(12), 1696–1709.
(3) Saunders, A. E.; Sigma, M. B.; Korgel, B. A. *J. Phys. Chem. B* **2004**, *108*, 193–199.
(4) Beale, A.; van der Eerden, A.; Jacques, S.; Leynaud, O.; O Brien, M.; Meneau, F.; Niketenko, S.; Bras, W.; Weckhuysen, W. *J. Am. Chem. Soc.* **2006**, *128*, 12386–12387.
(5) Jensen, H.; Bremholm, M.; Nielsen, P.; Joensen, K.; Pedersen, J.; Birkedal, H.; Chen, Y.; Almer, J.; Sogaard, E.; Iversen, S.; Iversen, B. *Angew. Chem., Int. Ed.* **2007**, *46*, 1113–1116.
(6) Abecassis, B.; Testard, F.; Spalla, O.; Barboux, P. *Nano Lett.* **2007**, *7*, 1723–1727.
(7) Biswas, K.; Varghese, N.; Rao, C. *J. Mater. Sci. Technol* **2008**, *24*, 615–627.
(8) Sakamoto, N.; Harada, M.; Hashimoto, T. *Macromolecules* **2006**, *39*, 1116–1124.
(9) Kimling, J.; Maier, M.; Okenve, B.; Kotaidis, V.; Ballot, H.; Plech, A. *J. Phys. Chem. B* **2006**, *110*, 15700–17707.
(10) Green, D.; Lin, J.; Lam, Y.; Hu, M.-C.; Schaefer, D.; Harris, M. *J. Colloid Interface Sci.* **2003**, *266*, 346–358.
(11) Marmiroli, B.; Grenci, G.; Cacho-Nerin, F.; Sartori, B.; Ferrari, E.; Laggner, P.; Businaro, L.; Amenitsch, H. *Lab Chip* **2009**, *9*, 2063–2069.
(12) Plech, A.; Kotaidis, V.; Siems, A.; Sztucki, M. *Phys. Chem. Chem. Phys.* **2008**, *10*, 3888–3894.
(13) Schmidt, W.; Bussian, P.; Linden, M.; Amenitsch, H.; Agren, P.; Tiemann, M.; Schuth, F. *J. Am. Chem. Soc.* **2010**, *132*, 6822–6826.
(14) Polte, J.; Ahner, T.; Delissen, F.; Sokolov, S.; Emmerling, F.; Thunemann, F.; Kraehnert, R. *J. Am. Chem. Soc.* **2010**, *132*, 1296–1301.
(15) Polte, J.; Emmerling, F.; Radtke, M.; Reinholz, U.; Riesemeier, H.; Thunemann, A. *Langmuir* **2010**, *26*, 5889–5894.
(16) Bolze, J.; Peng, B.; Dingenouts, N.; Panine, P.; Narayanan, T.; Ballauf, M. *Langmuir* **2002**, *18*, 8364–8369.
(17) Pontoni, D.; Narayanan, T.; Rennie, A. *Langmuir* **2002**, *18*, 56–59.
(18) Polte, J.; Erler, R.; Thunemann, A.; Sokolov, S.; Ahner, T.; Radermann, K.; Emmerling, F.; Kraehnert, R. *ACS Nano* **2010**, *4*, 1076–1082.

spectroscopy (XANES) can be used to follow the chemical state of atoms in solution with good time resolution.[19,20] Similarly, a recent publication reports on the mechanism of platinium nanoparticle formation probed at the single nanoparticle level by using in situ transmission electron microscopy (TEM) with a microfabricated liquid cell.[21]

The microscopic understanding of the nucleation phase and its further coupling with the growth phases are two main goals of active research. Several experimental achievements have been made to understand the nucleation and growth of many types of nanoparticles. Regarding AgBr, Sugimoto[22] formulated an expression for the final number density of particles with a continuous addition of monomers, using the classical nucleation theory (CNT). Leubner[23] used the balance between nucleation and growth processes to model synthesis of AgBr, AgCl, and AgI particles, but the very early stage of nucleation was not described. From a theoretical standpoint, Talapin et al.[24] completed the approach by following the evolution of an assembly of particles ruled by diffusion/reaction growth laws. Regarding metallic particles, Shevchenko et al.[25] related the final size of Co/Pt nanoparticles to their rate of nucleation. The basis of all these interpretations is the existence of a supersaturation in solution which determines the size of the nuclei. Another basis is a growth by monomer adhesion to the surface of growing nanoparticles. Using in situ UV−visible spectroscopy to measure the size and the shape of CdSe nanoparticles, Embden and Mulvaney[26] found that the experimental nucleation of CdSe nanoparticles with a hot injection method has to last long and cannot be described by a burst of nucleation. However, a more recent contribution of this group using a population balance equation coupled with CNT and growth law allows one to reproduce their experimental results,[27] showing that the growth was limited by surface reaction. Very recently, Rempel et al.[28] also proposed a model for semiconductor nanocrystals which captures the reactions underlying the nucleation and growth process. On the other hand, Kwon et al.[29] used a model based on nucleation and growth processes with a monomer supply step. This model can also describe the experimental results of a heating process for iron oxide nanocrystal formation reproducing the size and density number from the first nuclei to the final particles.[29] A global conclusion of many of these schemes is that the subtle balance between the rates of nucleation and growth limits the number of final particles.[25−27] Despite these thorough results, some drawbacks have not been addressed. For instance, in most cases, the initial distribution is fixed a priori (log-normal or Gaussian)[30,31] and not generated by a physical process.[30]

Comparison between theory and experimental data is scarce due to the lack of experimental data and particularly for very rapid systems. However, this lack of confrontation is not peculiar to the field of nanoparticles and is also reported in geochemistry when considering nucleation an growth of minerals[32] even at the geological time scale.[33,34] Therefore, there is still a strong need for experimental data to determine the key parameters of the nucleation and growth process of nanoparticles. Particularly, the influence of the feeding in monomer on the final size and shape of nanoparticles is generally not described. Moreover, althougth the role of the ligands is clear for the stabilization of the nanoparticles, our understanding of their role on the nucleation step has to be improved.[35]

Here, we present for the first time in situ XANES experiments with 100 ms time resolution to obtain the speciation of gold species (Au(III), Au(I), and Au(0)) from the beginning of the reaction (≃104 ms). This unique set of kinetic data on gold speciation with a high time resolution offers a nice opportunity toward the understanding of nucleation and growth of nanoparticles. Indeed, it can be combined with a time-resolved SAXS experiment,[6] which assesses in a quantitative fashion yields, radius, shape, and polydispersity of nanoparticles from the earliest instant of the reaction. The combination offers a comprehensive study on nucleation and growth of gold nanoparticles. A model is developed, by considering the variation of number, size, and shape of nuclei and nanoparticles induced by the formation of monomers in the solution. The confrontation with experiment allows identification of the main parameters controlling the final size distribution.

Materials and Methods

Synthesis. The experimental conditions are similar to those described in a former paper.[6] The gold nanoparticles are synthesized using a procedure described by Jana and Peng.[36] A solution containing the gold salt ($AuCl_3$, 0.007 M), solubilized in toluene by a cationic surfactant (didodecyldimethylammonium bromide, DDAB, 0.028 M), is mixed with a reducing solution containing the borohydride salt (tetrabutylammonium borohydride, TBAB, 0.028 M), DDAB (0.028M), and either decanoic acid or decylamine (0.1 M) as ligand in toluene.

In Situ XANES and SAXS. Two different experiments are combined in this work. The SAXS experiments were performed at the ESRF (European Synchrotron Radiation Facility, Grenoble, France) on the high brilliance ID-2 beamline. XANES at the L-III gold edge was recorded on the Dispersive EXAFS beamline (ODE) of the SOLEIL Synchrotron (Saint-Aubin, France). In both of these experiments, fast and reproducible turbulent mixing of the two precursor solutions (gold salt and reducing agent/ligand solutions) was achieved by using a stopped-flow setup (SFM 400, Bio-Logic).[37−39] Two different measuring cells were mounted on the head of the stopped-flow after the last mixer, ensuring that the kinetics of the reaction was exactly the same in the two setups. The cell for SAXS experiments was a classical quartz capillary of 1.5 mm path length. For the XANES experiment, due to the very low concentration of gold (a few millimolar), a dedicated cell with a path of 10 mm was built to ensure a complete jump of absorbance of 0.1 through the edge. A drawing of the cell can be found in the Supporting Information. Regarding

(19) Harada, M.; Inada, Y. *Langmuir* **2009**, *25*(11), 6049–6061.
(20) Chan, E.; Marcus, M. A.; Fakra, S.; ElNaggar, M.; Mathies, R. A.; Alivisatos, A. *J. Phys Chem A* **2007**, *111*, 12210–12215.
(21) Zheng, H.; Smith, R. K.; Jun, Y.; Kisielowski, C.; Alivisatos, A. *Science* **2009**, *324*, 1309–1312.
(22) Sugimoto, T. *J. Colloid Interface Sci.* **1992**, *150*, 208–225.
(23) Leubner, H. *J. Phys. Chem.* **1987**, *91*, 6069–6073.
(24) Talapin, D.; Rogach, A.; Haase, M.; Weller, H. *J. Phys. Chem. B* **2001**, *105*, 12278–12285.
(25) Shevchenko, E.; Talapin, D.; Schnablegger, H.; Kornowski, A.; Festin, R.; Svedlindh, P.; Haase, M.; Weller, H. *J. Am. Chem. Soc.* **2003**, *125*, 9090–9101.
(26) Embden, J.; Mulvaney, P. *Langmuir* **2005**, *21*, 10226–10233.
(27) van Embden, J.; Mulvaney, P. *J. Phys. Chem. C* **2009**, *113*, 16342–16355.
(28) Rempel, J.; Bawendi, M. G.; Jensen, K. *J. Am. Chem. Soc.* **2009**, *131*, 4479–4489.
(29) Kwon, S. G.; Park, J.; Hyeon, T. *J. Am. Chem. Soc.* **2007**, *129*, 12571–12584.
(30) Park, J.; Joo, J.; Gu, K. S.; Youngjin, J.; Taeghwan, H. *Angew. Chem.* **2007**, *46*, 4630–4660.
(31) De Smet, Y.; Deriemaeker, L.; Finsy, R. *Langmuir* **1997**, *13*, 6884–6888.
(32) Auer, D.; Frenkel, S. *Nature* **2001**, *409*, 1020.
(33) Noguera, C.; Fritz, B.; Clement, A.; Baronnet, A. *J. Cryst. Growth* **2006**, *297*, 180–186.
(34) Noguera, C.; Fritz, B.; Clement, A.; Baronnet, A. *J. Cryst. Growth* **2006**, *297*, 187–198.
(35) Gebauer, D.; Colfen, H.; Verch, A.; Antonietti, M. *Adv. Mater.* **2009**, *21*, 435–439.
(36) Jana, N.; Peng, X. *J. Am. Chem. Soc.* **2003**, *125*, 14280–14281.
(37) Ne, F.; Testard, F.; Zemb, T.; Grillo, I. *Langmuir* **2003**, *19*, 8503–8510.
(38) Weiss, T.; Narayanan, T.; Wolf, C.; Gradzielsky, M.; Panine, P.; Finet, S.; Helsby, W. *Phys. Rev. Lett.* **2005**, *94*, 38303.
(39) Panine, P.; Finet, S.; Weiss, T.; Narayanan, T. *Adv. Colloid Interface Sci.* **2006**, *127*, 9–18.

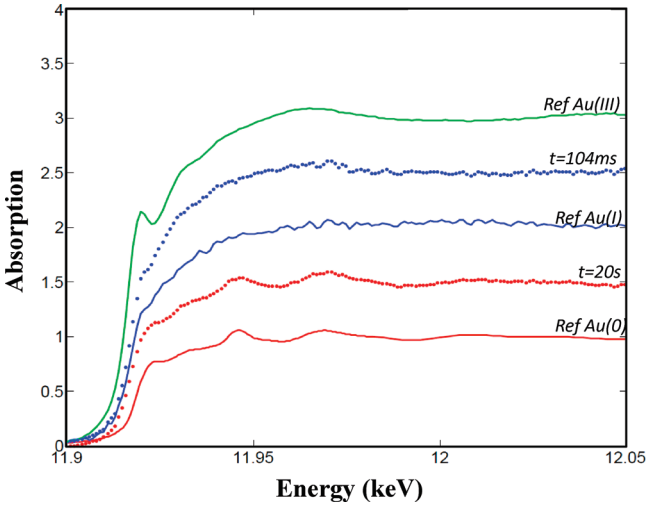

Figure 1. XANES spectra at the gold LIII edge for the synthesis of gold nanoparticles with the acid ligand. t = 104 ms corresponds to the average spectrum (normalized to 2.5 for clarity) recorded 104 ms after the mixing. t = 20s refers to the final spectrum (normalized to 1.5). Ref Au(III) is the spectrum of the initial gold(III) solution before the addition of a reducing agent (normalized to 3). Ref Au(I) is obtained after a mild reduction of the initial gold(III) solution (normalized to 2). Ref Au(0) is the spectrum obtained from a gold foil (normalized to 1).

SAXS, just after the mixing, a series of patterns was recorded with a delay of 80 ms between each series and an accumulation time of 50 ms. The data reduction procedure and the fitting of the scattering patterns to obtain the number density and the average radius of the particles with time have been presented in a previous paper.[6] In the case of XANES, the use of a dispersive setup allows one to reach a time resolution equal to the one of SAXS. The delay between the acquisition was 104 ms, and the accumulation time was 13 ms. However, in order to get an acceptable signal-to-noise ratio, the whole experiment was repeated up to 100 times and each spectra discussed hereafter at a given time represents an average over these repetitions. Before the kinetic experiment, we checked that when only the $AuCl_3$ solution was injected in the cell, no measurable reduction in Au(0) and particle formation was induced by the beam.

Results

Assessing the Gold Speciation with Time. The final nanoparticles are made of Au(0) atoms which come from the reduction of the initial Au(III) solution by a strong reducing agent BH_4^-. The rate of appearance of the Au(0) atoms is ruled by the chemical pathways by which the soluble Au(III) ions in solution are reduced. It can come either from a direct reduction of Au(III), from a reduction of Au(I) in bulk, or at the surface of the nanoparticles.[40]

Measuring the concentration of these species is mandatory to unravel the chemical pathways by which the nanoparticles appear. As the concentration of two of these species (Au(I) and Au(0)) cannot be measured by classical laboratory UV−visible spectroscopy, XANES was used to follow the concentration of all the gold species. Indeed, Au(III), Au(I), and Au(0) can be discriminated by XANES spectra at the L-III gold edge.

The three reference spectra are reported as lines in Figure 1. They were obtained as follows: the Au(III) spectrum comes from the initial $AuCl_3$ solution. A signature of this oxidation state is a prepeak at around 11.920 keV. The Au(0) spectrum was obtained from a gold foil. The spectrum shows two peaks, with the first one (at 11.945 keV) being directly linked to the electronic state. Finally, a solution of Au(I) in a toluene/DDAB solution was obtained by a mild reduction with ascorbic acid of the initial Au(III) salt solution. We have verified that the obtained spectrum is identical to that of a Au(I) salt powder (AuCl). The features of the Au(I) spectrum are less marked, since only a slight shoulder is seen at 11.925 keV. However, the lack of a peak at 11.920 and 11.945 keV allows one to separate it from Au(III) and Au(0).

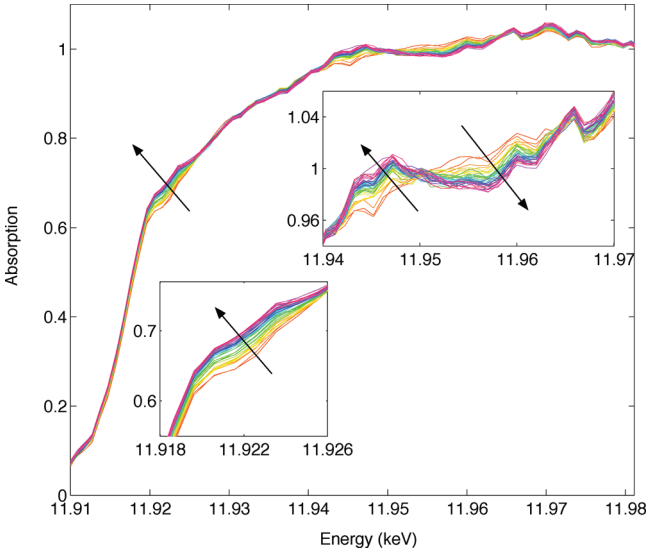

Figure 2. Time-resolved XANES spectra after mixing at the gold LIII edge for the synthesis of gold nanoparticles with the acid ligand. The arrows indicate the variation of the signal with increasing time. The first spectra was obtained 104 ms after the mixing. Only a few selected spectra are shown up to 10 s of reaction time, but one spectrum was registered every 117 ms. The spectra shown are an average over 100 repetitions of the experiment. The experimental jump of absorption (which is around 0.1) has been normalized to one. The absorbance shows two regions enlightened in the insets where the signal is changing when the reaction proceeds (from bottom to top at 11.922 keV, for example). These two regions are used to calculate the rate $\alpha(t)$ of transformation of Au(I) in Au(0).

During the gold nanoparticle synthesis, spectra were recorded every 104 ms after the rapid mixing. As can be seen in Figure 1, this initial spectrum (thus 104 ms after the mixing) is very close to the Au(I) reference. Hence, it does not share any of the features of either the Au(III) or the Au(0) spectra. After 104 ms, the gold atoms are all under the Au(I) form. On the other hand, at the end of the synthesis, the final spectrum (Figure 1) is close to the one of Au(0). Hence, from the speciation point of view, two reactions are observed. First, a rapid reduction of Au(III) in Au(I) occurs in less than 100 ms. Then, Au(I) is gradually transformed in Au(0).

Regarding the kinetic evolution, some selected spectra are shown in Figure 2 for the acid ligand case at 298 K. Defining at every time t after the mixing $\alpha(t)$ as the fraction of gold atoms under the oxidation state 0, the XANES absorbance (A) can be fitted as a linear combination of Au(0) and Au(I):

$$A(t) = (1-\alpha(t))A[\mathrm{Au(I)}] + \alpha(t)A[\mathrm{Au(0)}] \qquad (1)$$

In principle, the amplitude variation of the absorption at every energy E yields a measure of $\alpha(t)$. It is accurate for the energy channels with the most marked variation (insets in Figure 2). These energies are the ones corresponding to the peaks and valleys in the absorption spectra. For example, the absorption at 11.946 keV varies from 0.97 to 1.01. For each of these energy values, $\alpha(t)$ is

(40) Jana, N.; Gearheart, L.; Murphy, C. *J. Phys. Chem. B* **2001**, *105*, 4065–4067.

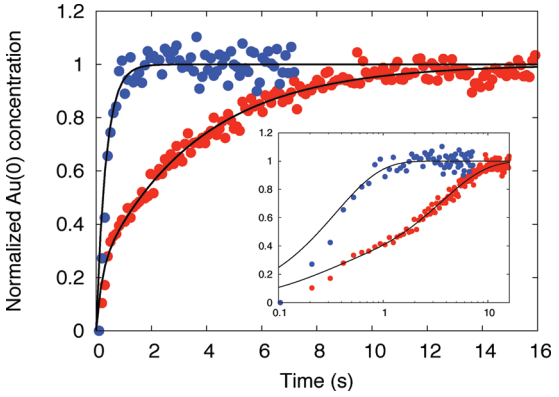

Figure 3. Formation rates of Au(0) for the acid ligand case (red) and amine ligand case (blue) at $T = 298$ K. The time resolution is 117 ms. The lines are the best fit obtained from eq 11 with the parameters in Table 1. These fits are further used in the model calculations. Time logarithm scale is shown in the inset.

obtained with a relative accuracy of 15%. Then, a final average over at least 30 relevant channels improves the relative accuracy on $\alpha(t)$ up to 5%.

The fraction $\alpha(t)$ includes the atoms Au(0) in the nanoparticles plus the ones which are still free in solution. The $\alpha(t)$ for the acid and amine ligand cases, normalized to their final value for comparison are reported in Figure 3. The nature of the ligand strongly influences the time dependence in a significant way. This is also observed for temperature. As it will be described in the following, these differences in the first instants of the reaction have important repercussions on the formation pathway of the particles.

Assessing Size Distribution during Nanoparticle Formation. As underlined in the Introduction, in situ SAXS experiments also provide, through the fitting of the scattering patterns at the absolute scale, the change in radius, dispersion, and concentration of gold nanoparticles from the formation of the first nucleus to the final state (see the Supporting Information for typical SAXS data and TEM images). Figure 4 shows the results for the two different ligands (acid and amine). As shown by Jana and Peng,[36] when the acid ligand is used, the particles have an average diameter (7 nm) much bigger than that with the amine ligand (3 nm) (see the Supporting Information). Understanding this ligand effect is one objective of this work. Using XANES, we have already shown that the rate of reduction of Au(I) in Au(0) is quicker for the amine ligand. On the other hand, the SAXS results (Figure 4) show that nucleation and growth are decoupled in time or happen simultaneously depending on the chemical nature of the ligand. When a carboxylic acid ligand is used, nucleation occurs first (a burst of nucleation is observed) and stops after 1 s as shown in Figure 4. Furthermore, the absence of an increase in the scattered intensity at low q showed that there is no further aggregation of the particles; the particles grow independently of the others and not by aggregation. More precisely, it was shown[6] that the nanoparticles then grow through a reaction limited mechanism yielding particles with approximately a 7 nm final diameter. It is also remarkable that the experimental curves have a maximum in particle number just after the burst of nucleation. In contrast, when an amine ligand is used, the nucleation time is much shorter and a higher quantity of monomers is consumed in this step. Consequently, we nearly do not observe any growth phase and the particles are smaller (around 2.6 nm in diameter).

In the acid ligand case, the reaction was analyzed for two other temperatures. We observed that an increase in temperature yields

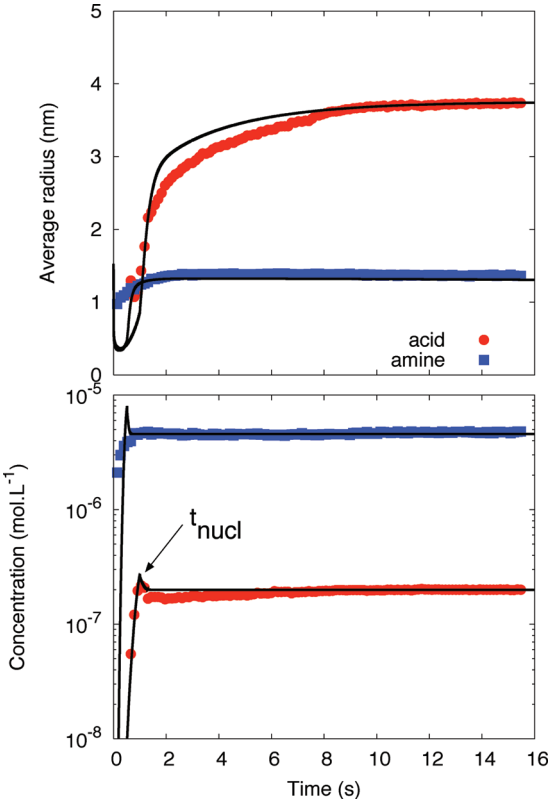

Figure 4. Effect of the ligands on the number density and radius obtained from fitting of in situ SAXS patterns: (red) acid ligand case and (blue) amine ligand case. The lines are the best fits obtained from the model described in the paper with the parameters in Table 2.

faster kinetics as reported in Figure 5. Generally, in bulk synthesis, a decrease of the size of the nanoparticle is observed with increasing temperature,[25,41] but Rao and Kalyanikutty[42] have observed an increase of the final size with increasing temperature for the synthesis of gold nanoparticles at the toluene−water interface. In the present case, the kinetics are faster and the particles are slightly bigger at higher temperature. The nucleation burst is even barely observable in the 318 K case. The final number of particles does not depend on temperature, and the separation between nucleation and growth is preserved on the studied temperature range. These experimental features with high time resolution can be quantitatively reproduced within the simple model that will be presented, allowing identifying key points of the mechanism of nanoparticles formation.

Assessing the Rate of Formation of Gold Nanoparticles. The rate of formation of nanoparticles (or yield) of the reaction α^{NP} at any time t is defined as the number of gold atoms in the nanoparticles n_t divided by the total number of initial gold ions n_{ini}[Au(III)]:

$$\alpha^{NP} = \frac{n_t}{n_{ini}[Au(III)]} \quad (2)$$

It can differ from the fraction $\alpha(t)$ obtained formely by XANES analysis, since it does not count the monomers or very small clusters. As previously shown,[6] α^{NP} can be obtained directly from the SAXS diagrams $I(q,t)$. Indeed, at any time t, the volume fraction of particles $\Phi_p = n_t$[Au(0)] × v_m (with v_m being the volume of

(41) Sugimoto, T. *Adv. Colloid Interface Sci.* **1987**, *28*, 65–108.
(42) Rao, C.; Kalyanikutty, K. *Acc. Chem. Res.* **2008**, *41*, 489–499.

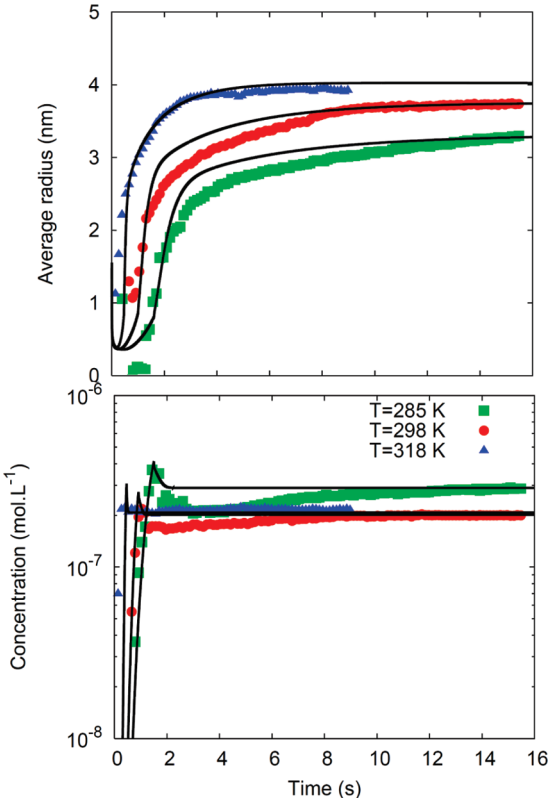

Figure 5. Temperature effect on the number and radius obtained from fitting of in situ SAXS patterns for the acid ligand case. The lines are the best fits obtained from the model described in the paper with the parameters in Table 2.

a gold atom in the solid phase) is calculated using the general property:

$$Q = \int_0^\infty I(q)\, q^2\, \mathrm{d}q = 2\pi^2(\Delta\rho)^2\Phi_p(1-\Phi_p) \qquad (3)$$

where $\Delta\rho$ is the scattering length density contrast between gold and toluene for X-rays. Q only depends on the volume fraction and contrast and is therefore called "invariant". The yield of nanoparticles α^{NP} obtained by SAXS can thus be compared to the total amount of Au(0) obtained by XANES for every time of reaction. The normalized values to the final Au(0) fraction for both XANES and SAXS results are compared in Figure 6 for the acid ligand case.

Discussion

Experimental Measurement of a Maximum of Supersaturation. The difference between the total amount of Au(0) (given by XANES) and the amount of Au(0) in nanoparticles (given by SAXS) is reported in Figure 6 (technically, the difference is done between the fit of the XANES result using the eq 11 and the data of the SAXS). A fascinating result is that the subtraction yields a measurable experimental concentration of free monomers of Au(0). This is a direct demonstration that gold atoms Au(0) exist in solution as monomers or very small clusters. Furthermore, the experimental concentration of monomers increases strongly during the nucleation period and passes through a maximum before decreasing back to a very low value. In parallel, as can be seen in Figure 4, a burst of nucleation occurs at t_{nucl} close to the maximum of concentration of monomers Au(0). This strong time correlation between a transient increase of gold Au(0) in solution and a burst of the number of particles is in direct agreement with

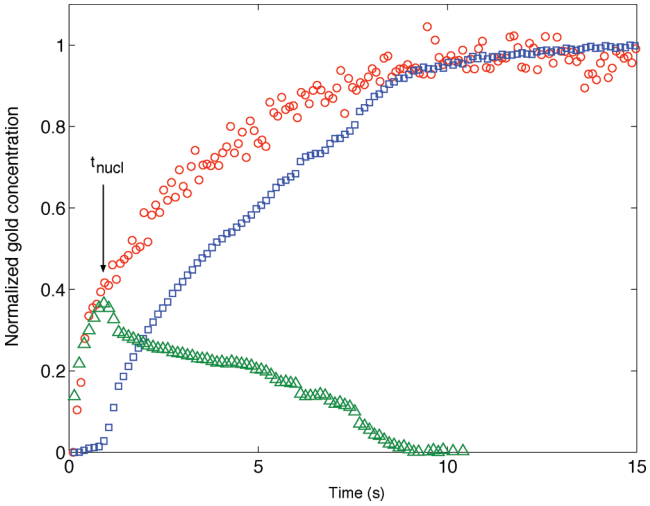

Figure 6. Formation rate of monomers for the acid ligand case at $T = 298$ K (circle) from XANES. Yield of reaction (square) from SAXS; free gold atoms Au(0) (triangle) obtained by the difference between the formation rate of monomers (fitted with the eq 11) and the yield of reaction.

the old Lamer scheme.[43] This calls for a model where the increase in concentration of monomers Au(0) is coupled with the nucleation and growth equations.

Nucleation and Growth Model. In order to get a comprehensive view of the formation mechanism from the formation rate of Au(0) to the final size distribution, each particle can be treated as nucleating and growing (or dissolving) in a feeding solution of monomers. This last assumption is supported by the results shown in the experimental part. The constant number density of particles after the initial burst of nucleation strongly evidences that the particles grow independently of the others and not by aggregation, contrarily to the classical reduction by citrate for which a first initial aggregation stage has been observed.[14] This implies that a process of feeding by monomers has to be involved. Guided by the different experimental results, a model comprising the formation rate of Au(0), nucleation, and growth as the three elementary processes is developed and compared to the experiments.

The concentration with time of atoms Au(0) is known as the formation rate. From a structural standpoint, the assembly of Au(0) can be divided, at any time, into two populations: the ones which are free in solution and the ones included in the nanoparticles. Three processes occur concomitantly: formation of new monomers through reduction of the precursors (either in bulk or at the surface), nucleation of new particles, and growth of the existing particles. With a partial molar volume of v_m, a total volume fraction of formed gold monomers can be defined and is denoted Φ_i. For a given supersaturation S, the rate of nucleation, the initial radius (volume) of the nuclei are denoted J_+, r_c (v_c), respectively. Similarly to J_+, one can define a rate of total dissolution J_- of particles reaching a minimum radius (volume) r_0 (v_0) during the course of their evolution. The assembly of growing nanoparticles can be described by an evolving number density distribution function in radius $N(r,t)$ yielding a total volume fraction of particles:

$$\Phi_p(t) = \int N(r,t)\, v(r,t)\, \mathrm{d}r \qquad (4)$$

(43) Lamer, V. K.; Dinegar, R. H. *J. Am. Chem. Soc.* **1950**, *72*, 4847–4854.

The supersaturation of the solution can then be defined as

$$S(t) = \frac{\Phi_i - \Phi_p}{\Phi_{eq}} \quad (5)$$

where Φ_{eq} is the equilibrium solubility of a gold macroscopic surface in the solvent. The evolution of the supersaturation S with time is then linked to the three processes in parallel.

Up to now, the proposed scheme only contains the conservation of matter. Going further imposes to detail three terms, that is, the nucleation rate J_+, the initial size of the nuclei r_c, and a growth law. The clear experimental correlation between the maximum in free Au(0) and nucleation supports the hypothesis that the monomers are the Au(0) atoms (or very small clusters of them) free in solution. Different forms of the relation between J_+ and n_t[Au(0)] (or the instantaneous supersaturation $S(t)$) can be chosen. We chose the most classical one proposed by the classical nucleation theory:[44,45]

$$J_+ = \beta^* \Phi_i \, e^{-\frac{\Delta G_c}{kT}} \quad (6)$$

with

$$\frac{\Delta G_c}{kT} = \frac{16\pi\gamma^3 v_m^2}{3(kT)^3} \frac{1}{\log^2(S)} \quad (7)$$

and γ being the surface tension of the solid/liquid interface and β^* the efficiency of the collision rate. It is worth noting that if $\Delta G_c/kT$ is low, eq 6 reduces to a first order reaction for the nucleation. Finally, CNT also offers a link between the critical nuclei radius and the supersaturation:

$$r_c = \frac{2\gamma v_m}{kT \log(S)} \quad (8)$$

Regarding the growth term, classical models have shown that the rate of increase of the volume of a particle of size r, $\dot{v}(r) = dv(r)/dt$, can be linked to the supersaturation through[24]

$$\dot{v}(r) = 4\pi r^2 K \Phi_{eq} \frac{(S - e^{r^*/r})}{(Kr)/D + 1} \quad (9)$$

In eq 9, when the growth is limited by diffusion, $Kr/D \gg 1$ (with D in $nm^2 s^{-1}$ being the diffusion coefficient of the monomer), meanwhile when the growth is limited by surface reaction, $Kr/D \ll 1$ with K being the surface reaction constant (in $nm \cdot s^{-1}$). Equation 9 also indicates that the rate of change of the radius depends on the supersaturation. In particular, it can become negative when $S < e^{r^*/r}$ and the size can decrease. One can observe that, with v_m and $\phi_i(t)$ known, the parameters to describe the kinetic behavior of the system are γ, Φ_{eq}, β^*, and K. Some fundamental features produced by the calculation are given in the Supporting Information.

The quantity containing all the information on the system and that we aim to get as an output of the calculation is $N(r,t)$. The resolution scheme is based on the step by step formation of monomers. For each incremental step of time δt, three operations are performed. First, the number of new particles $\delta N = J_+ \delta t$ is calculated together with their radius which is taken as the instantaneous critical radius r_c. Hence, at each step n, a new family is created. Then, the former families are allowed to grow using eq 9. Note that the new family has by construction an initial rate of growth which is zero. As a third step, the mass conservation allows one to define the new supersaturation for the next cycle. After n cycles, one handles an ensemble (F_n) of n families of particles. The distribution of the families' radius $N(r,t)$ can be calculated from (F_n) at any time of the resolution. Finally, it is worth noting that the model does not consider any secondary aggregation i.e. the particles can only grow or dissolve. This is related to the role attributed to the ligands present in solution, which is to stabilize the particles against a secondary aggregation. This procedure is very close to the one used by Noguera et al.;[33,34] however, the main difference is that a formation rate is incorporated in the present case. Finally, one can get the average radius with time, together with the number density:

$$N_p(t) = \int N(r,t)\, dr \quad (10)$$

and the supersaturation S. These numbers can be compared to the measured ones.

Table 1. Results for the Fits of the Formation Rates[a]

ligands	amine ligand	acid ligand	acid ligand	acid ligand
T	298	298	285	318
τ_1 (s)	0.3	0.2	**0.3**	
τ_2 (s)		3.6	**5**	1.6
B	1	0.22	**0.3**	0

[a] The values in bold were not measured by fitting the experimental rates but deduced from the best fitting of radius and number density with time.

Comparison with Experiment for the Acid Ligand Case. An important ingredient of the model is the feeding of monomers, also called the formation rate of monomers. In the present synthesis, the total amount of Au(0) atoms injected by the two successive chemical pathways is at any time followed by XANES. In order to be introduced in the resolution scheme of the model, the normalized fraction of Au(0) measured by XANES was fitted using a simple phenomenological law combining two exponential regimes:

$$\frac{\alpha}{\alpha_f} = B(1 - e^{-t/\tau_1}) + (1 - B)(1 - e^{-t/\tau_2}) \quad (11)$$

The different values obtained for the fitting parameters are reported in Table 1 for the different cases.

The resolution of the *monomer formation/particle nucleation–growth* model was first considered for the acid ligand case. With the formation rate of monomers established, only four unknown parameters (K, γ, S_{max}, and β^*) are required for the model (with S_{max} being the maximum potential supersaturation if all the momomers were injected instantaneously). It is not possible to assess experimentally the solubility of gold Au(0) in toluene in the presence of DDAB or the interfacial energy. Hence, the couple (γ,S_{max}) was not known initially.

A first conclusion comes from the structure of the different equations where γ and log(S) appear. While the dependence on γ was very high, the dependence on S_{max} was weak, provided it was high enough. We thus fixed S_{max} to 4000 in the following discussion. For a given pair (γ,S_{max}), the best values of β^* and K were determined by fitting two important characteristics of the data: the final number of particles and the time position of the burst of nucleation (t_{nucl}). This process always imposed a unique couple (β^*,K).

Two sets of parameters yielding good fits have been selected for discussion and are reported in Table 2 for the acid ligand case at 298 K. Taking $\gamma = 0.2862\ J \cdot m^{-2}$ coupled with S_{max}, the fit yielded $K = 4 \times 10^{-4} m \cdot s^{-1}$ and $\beta^* = 10^{39}\ m^{-3} \cdot s^{-1}$. However, taking $\gamma = 0.1700\ J \cdot m^{-2}$ for the same $S_{max} = 4000$, a good fit was also obtained for $K = 4 \times 10^{-4}\ m \cdot s^{-1}$ and $\beta^* = 3.11 \times 10^{28}\ m^{-3} \cdot s^{-1}$. The two sets of parameters are quite different; however, three

(44) Kashchiev, D. *Nucleation:Basic Theory with Applications*; Butterwoth-Heinemann: Oxford, 2000.
(45) Kaschiev, D. *J. Chem. Phys.* **2006**, *125*, 44505.

Table 2. Results for the Fits of the Radius and Number Density[a]

T	298	298	285	318
ligands	amine ligand	acid ligand	acid ligand	acid ligand
K ($m \cdot s^{-1}$)	2.2×10^{-4}	4×10^{-4}	1.7×10^{-4}	18.5×10^{-4}
β^* ($m^{-3} \cdot s^{-1}$)	1×10^{39}	$1.\ 10^{39}$ (3.1×10^{28})	1×10^{39}	1×10^{39}
γ ($J \cdot m^{-2}$)	0.2858	0.2862 (0.17)	0.2792	0.2858
S_{max}	4000	4000	4000	4000

[a] The two other fixed physical values were $v_m = 1.72 \times 10^{-29}$ m^3 and $D = 3.610^{-9}$ $m^2 \cdot s^{-1}$.

remarkable points have to be noted. First, the rate of growth K is the same for the two fits, and since $K/(Dr) \gg 1$, it reveals that the growth is limited by the surface reaction and not by the diffusion of monomer toward the surface of the growing particles. This reaction limitation was already noted by Saunders et al. for another gold nanoparticle production.[3] The second point pertains to the size of the first stable nuclei. In the two calculations, the maximum supersaturation reached during the reaction is around 1500, far below S_{max} as shown in the Supporting Information. Therefore, one can calculate, at t_{nucl} where the critical free energy is minimal and the nucleation maximum (burst), the minimal mass of the nuclei. This yields 2 atoms for $\gamma = 0.1700$ $J \cdot m^{-2}$ and 9 atoms for $\gamma = 0.2862$ $J \cdot m^{-2}$, more realistic values. A third related point is that the burst of nucleation is perfectly reproduced and also very close to the maximum of monomers concentration. It is remarkable that the burst in concentration can be reproduced. The fit also predicts a slight decrease in concentration just after the burst of nucleation. This phenomenon is also experimentally observed for the other conditions (see the effect of temperature); however, the weak re-increase in number afterward, which is observed experimentally and is not predicted, and the radius are not perfectly fit during the growth phase. These discrepancies can have several origins, all certainly linked to the approximations done in the nucleation and growth equations, such as spherical shape nuclei and size independent surface tension γ, simple models for the growth phase. Finally, taking $\gamma = 0.2862$ $J \cdot m^{-2}$, one obtains $\Delta G_c \simeq 80$ $kJ \cdot mol^{-1}$ (32 kT) at t_{nucl}. This shows that the exponential term in eq 6 for the nucleation rate cannot be neglected.

The prefactor β^* can further be compared to theoretical expectations in the framework of the homogeneous nucleation:

$$\beta^* = \frac{4\pi D r_c}{v_m v_{sol}} \tag{12}$$

where D is the coefficient of diffusion of a monomer and v_{sol} is the volume of the solvent molecule. This leads to $\beta^* = 10^{39}$ $m^{-3} \cdot s^{-1}$ which is of the same order of magnitude as the one with the bigger critical nuclei of 9 atoms. This indicates that the value of the homogeneous nucleation coefficient is also potentially valid in the present case of gold nanoparticle synthesis.

Influence of the Nature of the Ligand. Going to the amine ligand case at 298 K, the formation rate of monomers is much quicker as shown in Figure 3 and Table 1. Taking the faster formation into account in the model is almost enough to reproduce the experimental data for particle numbers and size if one takes all the same parameters as in the acid ligand case. Indeed, taking a constant supersaturation $S_{max} = 4000$ and $\gamma = 0.2858$ $N \cdot m^{-1}$, a good fitting requires only a slight decrease of the surface reaction constant K from 4×10^{-4} $m \cdot s^{-1}$ in the acid ligand case to 2.2×10^{-4} $m \cdot s^{-1}$ in the amine ligand case. An important conclusion is that the stabilizing ligand controls the size of the nanoparticles by controlling the formation rate of monomers. However, the molecular mechanism at play which could yield these differences remains difficult to assess rigorously. A possibility is that the acidic character of the carboxylic head makes it prone to react with the reducing agent (a borohydride) to yield (tri)acyloxyborohydride[46] as already suggested in our previous article. The reducing agent activity is reduced, and this impacts the feeding in monomers by slowing it drastically. More generally, this result shows that the control of the formation rate of monomers is a key point in the nanoparticles synthesis.

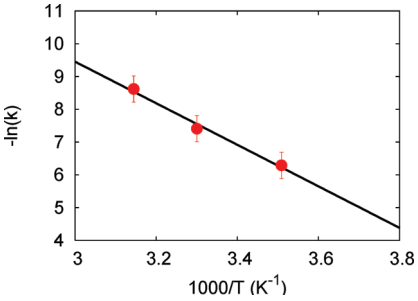

Figure 7. Growth rate constant K versus temperature, with K being obtained from the model and experimental curves of both concentration and radius of nanoparticles as shown in Figure 5.

Influence of Temperature. The influence of temperature can also be recovered by the model as reported in Figure 5, using the experimental formation rates of monomers for the cases at 298 and 318 K. The formation is more rapid at 318 K than at 298 K. For the 285 K case, the formation rate could not be measured experimentally and the parameters were deduced from the two other conditions of temperature as can be seen in Table 1. In order to reproduce the data, the surface tension had to be slightly adjusted to $\gamma = 0.2792$ $N \cdot m^{-1}$, which may not be significant due to the approximated formation rate. The rate of growth K has to increase from 1.7×10^{-4} to 18.5×10^{-4} $m \cdot s^{-1}$ when going from 285 to 318 K. Gathering the values of the growth constant for the different temperatures, we can define an activation energy for the limiting step of growth which is surface reaction:

$$K = K_0 \, e^{-\Delta G_c'/RT} \tag{13}$$

From a linear fit of the K versus $1/T$ data (Figure 7), we extract $\Delta G_c' = 52$ $kJ \cdot mol^{-1}$. The two energy barriers (nucleation and growth) are thus of the same order of magnitude. This supports the idea of a balance effect between nucleation and growth of nanoparticles. When increasing temperature, the nucleation becomes faster and this yields a larger amount of nuclei per unit time. On the other hand, the growth of these nuclei which hinders nucleation by consuming monomer is also faster. As a consequence, the nucleation phase is shorter but the final number and thus radius are less dependent on the temperature.

Conclusion and Perspectives

In summary, we assessed in situ and quantitatively the fast formation process of gold nanoparticles in solution. Combining XANES, SAXS, and a fast mixing device, we shed light on both the molecular processes occurring during the first instants of the reaction and on the nucleation and growth of the particles. An important result of these experiments is that during the reduction of Au(I) a measurable amount of Au(0) appears in bulk which shows that the model of a supersaturation of bulk monomer can be used. Furthermore, we show that the rate at which the monomer appears is the key point that controls the balance between the nucleation and the growth phases. For rapid systems, this rate is highly sensitive to the chemical nature of the ligand and to temperature. Finally, we compared these experimental results to a model which couples formation rate, growth, and nucleation

(46) Gribble, G. W. *Chem. Soc. Rev.* **1998**, *27*, 395–404.

laws. It catches the essential part of the phenomenom we experimentally observed and proves to be efficient in reproducing quantitative data, once the formation law is known. Consequently, one can predict that further progress in nanoparticle chemistry will certainly come from a finer control (and measure) of the formation of monomers. The methodology developed here could be extended to other chemical systems with the long-term intent to control more accurately the processes at play during the formation of a broader class of nanoparticles. This will inevitably lead to a finer control over the experimental conditions and hence to more straightforward discovery and optimization strategies. To do so, one has to disentangle purely chemical processes at the precursor level and more physical phenomena related to the formation and evolution of a solid phase in a liquid media. Though ubiquitous in several fields of science, the latter issue still remains poorly understood and experiments such as the ones presented here represent, in our opinion, a step toward this goal.

Acknowledgment. This work benefited from access to the ID2 beamline at the ESRF and ODE beamline at SOLEIL. From ESRF, we thank Stéphanie Finet for local contact during the experiments on the ID2 beamline and Teyencheri Narayanan for valuable discussions and comments. We particularly would like to thank Patrick Haltebourg for the design and making of the XANES cell, Olivier Tache for the control command scheme during time-resolved experiments, Philippe Barboux to have introduced us to the XANES field, and Antoine Thill for stimulating discussions during the interpretation and modelization. Finally, we would like to thank Matt Luchette for proofreading of the manuscript.

Supporting Information Available: Additional experimental details; discussion of supersaturation and distribution. This material is available free of charge via the Internet at http://pubs.acs.org.